

# Shape-Controlled Electroless Plating of Hetero-Nanostructures: AgCu and AgNi-decorated Ag Nanoplates on Carbon Fibers as catalyst for Oxygen Evolution Reaction

Patrick Bräuer<sup>\*,c</sup>, Falk Muench<sup>\*,c</sup>, Sasho Stojkovic<sup>j</sup>, Siddharth Gupta<sup>b</sup>, Matthew T. Mayer<sup>b</sup>, Wolfgang Ensinger<sup>c</sup>, Christina Roth<sup>d</sup>, Gumaa A. El-Nagar<sup>\*,a,b</sup>

<sup>a</sup>Department of Chemistry, Faculty of Science, Cairo University, Giza 12613, Egypt. (Gumaa A. El-Nagar)

<sup>b</sup>Helmholtz Young Investigator Group: Electrochemical Conversion, Helmholtz-Zentrum Berlin für Materialien und Energie GmbH, Hahn-Meitner-Platz 1, D-14109, Berlin, Germany. (G. A. El-Nagar, S. Stojkovic, S. Gupta & M. T. Mayer)

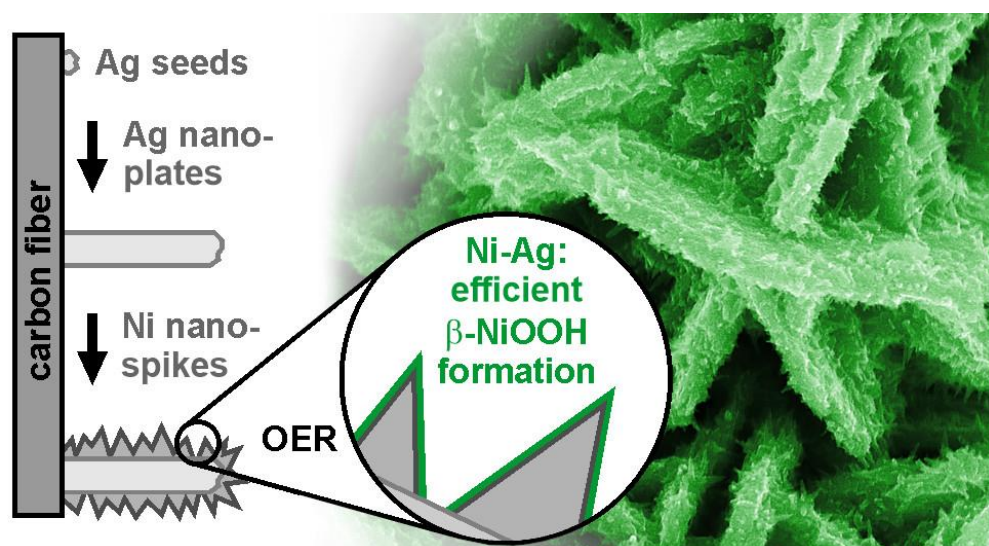
<sup>c</sup>Department of Materials and Earth Sciences, Technische Universität Darmstadt, Alarich-Weiss-Straße 2, D-64287, Darmstadt, Germany. (F.Muench, P. Bräuer & W. Ensinger)

<sup>d</sup> Electrochemical Process Engineering, Faculty of Engineering University of Bayreuth, D-95447 Bayreuth, Germany. (C. Roth)

**\*Corresponding authors:** G. A. El-Nagar ([Gumaa.el-nagar@helmholtz-berlin.de](mailto:Gumaa.el-nagar@helmholtz-berlin.de)) & Patrick Bräuer ([braeuer@ma.tu-darmstadt.de](mailto:braeuer@ma.tu-darmstadt.de)). <sup>\*</sup>shared first author

## ABSTRACT

This study addresses the potential of combining multiple electroless plating reactions for homogenous decoration of three-dimensional carbon fibers (CFs) with shape-controlled AgNi and AgCu bimetallic nanostructures. Morphology, crystal structure and composition of the obtained bimetallic nanostructures were systemically examined by various spectroscopic and microscopic techniques including SEM, TEM, XRD and XPS. The electrocatalytic performance of the synthesised materials was investigated for the oxygen evolution reaction. AgCu and AgNi bimetallic surfaces showed superior activity and stability compared to pristine Ag, Ni, or Cu. These observed enhancements on the bimetallic nanostructures are attributed to the synergistic effect between the elements present. AgNi nanoplates decorated CFs exhibited the highest activity towards oxygen evolution reaction (OER) which is attributed to the key role of Ag in stabilizing and increasing the number of  $\beta$ -NiOOH surface sites, which are the most relevant OER active Ni species.



**Keywords:** Electroless plating, oxygen evolution reaction, silver nanoplatelets, bimetallic nanostructures, water electrolysis

Department of Chemistry, Faculty of Science, Cairo University, Giza 12613, Egypt. (Gumaa A. El-Nagar)

## INTRODUCTION

Electrocatalytic water splitting is a promising strategy towards sustainable fuel production. However, the high overpotential and sluggish kinetics of the oxygen evolution reaction remains a key challenge and a major bottleneck in water electrolysis. Thus, designing efficient electrocatalyst materials for OER, providing good activity and satisfactory extended lifetime under operating conditions, is urgently required<sup>1,2</sup>.

Iridium and ruthenium-based oxides are the state-of-the-art electrocatalysts for OER due to their benchmark OER performance, and chemical compatibility in both acidic and alkaline conditions.<sup>3-4</sup> Unfortunately, their mass production is limited by their scarcity and high cost. Thus, the development of earth-abundant electrocatalysts with comparable OER performance is a critical need. Much effort has been dedicated to exploring the use of various non-precious transition metals including nickel, cobalt, iron, and copper, as well as their alloys, oxides, (oxy)hydroxides, sulfides, phosphides and nitrides as promising alternative OER electrocatalysts.<sup>1, 5-8</sup> Surface nanostructuring and defect engineering are considered effective strategies for improving OER performance via creating surfaces with high densities of electrochemically active surface sites.<sup>9-12</sup>

Apart from the compositional optimization, the development of facile, flexible, and directed synthesis approaches allowing the efficient fabrication of catalysts with a well-defined shape and composition is of great importance.<sup>13-14</sup> An extensive pool of different synthesis methods for tailoring of nanostructured materials with controlled morphologies has been developed in the past decades. However, the poor industrial applicability of many of those techniques from upscaling point of view is a serious issue. For instance, while vapor deposition strategies (e.g., sputter deposition and atomic layer deposition) represent valuable tools for creating functional coatings and nanomaterials, they are technologically demanding. Moreover, atomic layer deposition involves complex and expensive precursors, while sputtering suffers from poor conformality and problems with uniformly coating complex shaped work pieces attributing to the shadowing effect. Furthermore, both suffer from comparably low deposition rates.<sup>15</sup>

On the other hand, wet-chemical approaches, such as chemical bath deposition, electrodeposition, or electroless plating, tend to be simpler, well-suited to coat large complex surfaces, and more easily scalable.<sup>16-17</sup> Electroless plating shows an advantageous combination of characteristics, including excellent conformality,<sup>18-19</sup> the ability to coat non-conducting surfaces,<sup>18-19</sup> control over the deposit nanostructure and crystallinity,<sup>20-22</sup> and a straightforward autocatalytic growth mode just requiring the immersion of a substrate in a plating solution.<sup>23</sup> These characteristics make electroless plating a valuable technique for efficiently synthesizing nanomaterials.

In order to create complex nano-architectures and low-dimensional nanostructures, the replication ability of electroless plating is commonly used in conjunction with templating.<sup>18-19, 24-25</sup> However, the additional fabrication steps required for the production and optional removal of templates affect the simplicity, material cost and atomic economy of the overall process. As one approach to streamline materials synthesis and obtain well-defined nanostructures, we are developing shape-controlled electroless plating variants, which utilize strategies such as symmetry breaking and directed growth instead of templates to guide the formation of anisotropic products such as nanoplates, nanospikes or nanowires.<sup>21-22, 26</sup>

In this work, we explore the potential of combining multiple electroless plating reactions for creating functional coatings composed of hetero nanostructures. To this end, we utilize the

shape-controlled deposition of jagged silver nanoplates, which represent a promising platform for (electro)catalytic applications,<sup>21</sup> with the aim to fabricate a conductive, highly porous, micro- and nanostructured support layer. The nanoplates are then electrolessly decorated with two earth-abundant catalyst materials interesting for the OER, namely nickel,<sup>6</sup> and copper.<sup>12</sup> In this way, hierarchical multicomponent coatings can be directly grown on three-dimensional electrodes using a sequence of facile wet-chemical reactions. The performance of the obtained bimetallic silver-based nanostructured materials with controlled nanoplate-like structures were further investigated towards OER. Various microscopic and spectroscopic techniques combined with electrochemical methods were used to correlate the obtained good activity and durability of the bimetallic surface with their structure and composition.

## EXPERIMENTAL

### CHEMICALS

Ultrapure water, prepared from ion-exchanged water using a Milli-Q unit, > 18 M $\Omega$ ·cm<sup>-1</sup> at room temperature, was used in all experiments. The following chemicals were used as-received without further purification: Acetone (Fischer, techn.); AgNO<sub>3</sub> (Honeywell, ACS  $\geq$ 99.0%); CuSO<sub>4</sub>·5H<sub>2</sub>O (Sigma-Aldrich,  $\geq$ 98,0%); ethanol (VWR Chemicals, 99.8%); ethylenediamine (Sigma-Aldrich,  $\geq$ 99.0%); Fe(NO<sub>3</sub>)<sub>3</sub>·9H<sub>2</sub>O (Sigma-Aldrich,  $\geq$ 98,0%); 37% HCl(aq) (AppliChem, p.a.); 65% HNO<sub>3</sub>(aq) (AppliChem, p.a.); 80% N<sub>2</sub>H<sub>4</sub>(aq) (Merck, for synthesis); iminodiacetic acid (Fluka Analytical,  $\geq$ 98%); 30-33% NH<sub>3</sub>(aq) (Sigma-Aldrich, puriss.); NiSO<sub>4</sub>·7H<sub>2</sub>O (Acros Organics, p.a.); SnCl<sub>2</sub>·2H<sub>2</sub>O (Sigma-Aldrich, 98%); 32% NaOH(aq) (Sigma-Aldrich), sodium potassium tartarate tetrahydrate (Sigma-Aldrich,  $\geq$ 99%); NaOH (Sigma-Aldrich,  $\geq$ 98%); Pb(NO<sub>3</sub>)<sub>2</sub> (Sigma-Aldrich,  $\geq$ 99.0%); 37% formaldehyde in H<sub>2</sub>O (Sigma-Aldrich, ACS reagent, stabilized with 10-15 MeOH).

### CATALYST PREPARATION: CARBON FELT FUNCTIONALIZATION

Battery-type graphite felt (SGL Group, Sigracell GFA 6 EA) was cut into squares of approximately 2 cm x 2 cm size, cleaned with acetone, thoroughly rinsed with water, boiled in fresh *aqua regia* (3:1 HCl:HNO<sub>3</sub>) for 3 min, and washed again with water. Prior to being transferred to any of the four employed reaction solutions (sensitization, activation, plating, decoration), the water-washed carbon felt was briefly put onto a tissue paper to remove the excess water while avoiding a complete drying of the fibers. This allows the respective reaction solution to quickly permeate the whole felt including its inner surfaces, thus promoting deposit conformity. Avoiding drying and quick transfer also preserves the desired state of reactants such as adsorbed Sn<sup>2+</sup>, which is susceptible towards oxidation to Sn<sup>4+</sup>.

The seeding reaction proceeded in two steps. First, the felt was submerged in a sensitization solution (20 mM SnCl<sub>2</sub>, dissolved in an ethanol-water mixture (1:1 by volume) containing 100 mM HCl). The felt was stored in the solution for 30 min, washed with an ethanol-water mixture (1:1 by volume), and thoroughly rinsed with water. Then, the sensitized felt was submerged in an activation solution (20 mM AgNO<sub>3</sub> dissolved in water containing 80 mM NH<sub>3</sub>) for 3 min, and then thoroughly rinsed with water.

Silver nanoplates were grown on the seeded felt by submerging it in an electroless plating bath for ~1 h. The plating bath was obtained by first mixing equal volume parts of a reducing solution (240 mM sodium potassium tartrate in water) and a metal complex solution (40 mM AgNO<sub>3</sub>,

12 mM HNO<sub>3</sub> and 200 mM NH<sub>3</sub> in water), followed by adding 12.5 mM Fe(NO<sub>3</sub>)<sub>3</sub> and heating to 75 °C on a hot plate. Afterwards, the decorated felt with silver nanoplates was thoroughly washed with water to remove precipitates. Ag seeding step is important for homogeneous coating of the carbon fiber since they act as the autocatalytic surface where the reduction takes place. Having no Ag seeds on the carbon fibers ends up either with low coverage density or no coverage at all (see the below attached SEM images). As a result, the seeding step and aqua regia treatment are highly recommended for this way of synthesis (Figure S1).

Nanoplate decoration with Cu or Ni was achieved by applying a second electroless plating step. For the Cu plating bath, equal volume parts of a reducing solution (2 M formaldehyde in water) and a metal complex solution (460 mM sodium potassium tartrate, 480 mM ethylenediamine (en), 520 mM NaOH, 200 mM CuSO<sub>4</sub>) were mixed. Cu deposition proceeded by immersing the felt in the plating bath, transferring it to an oil bath at 40 °C, and waiting for a color change to dark reddish-brown (~7 min). The Ni plating bath was assembled by adding 1 M N<sub>2</sub>H<sub>4</sub>(aq) to a metal complex solution (40 mM NiSO<sub>4</sub>, 80 mM iminodiacetic acid (IDA) and 210 mM NaOH in water) at room temperature. Plating was performed at 70-75°C until the color of the felt changed to black (~25 min). After nanoplate modification, the felts were thoroughly washed with water and dried in air.

Control samples for the pure functionalizing metals (Ni and Cu) have been prepared by submerging carbon felt into the corresponding electroless plating baths. To initiate the plating reaction the carbon felt was coated in short term electrodeposition (30 sec at - 1V vs. Ag|AgCl, Pt Counter electrode) within the plating bath to create a seeding layer. Electroless plating was done subsequently as aforementioned.

## CHARACTERIZATION

Morphology, bulk composition, and elemental mapping of the as-prepared materials were examined by a scanning electron microscope (SEM, Philips XL30 FEG, 10 kV acceleration voltage) equipped with an energy dispersive X-ray spectrometer (EDS, EDAX XL30 CDU LEAP detector), and a transmission electron microscope (TEM, FEI CM20, 200 kV acceleration voltage, LaB<sub>6</sub> cathode). For TEM measurements, the as synthesized catalysts were embedded in a resin matrix and cut into thin layers (70 nm in thickness) to create an easily accessible cross-section of the hierarchical structure. The crystal structure of the synthesized catalyst materials was investigated by X-ray diffraction (XRD) in transmission geometry with Cu K<sub>α</sub> radiation ( $\lambda=1.54 \text{ \AA}$ ) using a STOE STADI-P diffractometer with a position sensitive detector. The X-Ray photoelectron spectroscopy (XPS) measurements were conducted with a SPECS Phoibos HSA3500 100 instrument with a monochromatic Al K<sub>α</sub> X-ray source (1486.74 eV). The XPS spectra were measured as survey and high resolution for the Ni 2p, Cu 2p, Ag 3d and O 1s core levels, before and after OER electrocatalysis. The high-resolution spectra peak positions were calibrated with respect to the adventitious carbon - C 1s peak at 284.8 eV that is attributed to C-C bond. The deconvolution and fitting of the high-resolution spectra were performed using the XPS PeakFit software. Ni 2p fitting parameters were taken from Biesinger et al.<sup>27</sup> For characterization of the samples after the OER electrocatalysis, we established a glovebox assisted XPS setup (*quasi in situ* XPS). Briefly, prior to the XPS characterization, the electrochemical experiments were conducted in a glovebox under inert atmosphere (purged with N<sub>2</sub>). The samples were transferred under inert conditions using an accordingly designed transfer module to the XPS instrument.

## ELECTROCHEMISTRY

The electrochemical experiments were carried out in a three-electrode electrochemical setup using a Gamry potentiostat/galvanostat (Reference 3000) at room temperature. Coated carbon felts (spherical piece with diameter of 0.7 cm) with bimetallic AgNi and AgCu and pristine Ni, Cu and Ag nanoplates pieces (spherical, diameter 0.7 cm) pierced with a glassy carbon rod were used as working electrodes. The current density was calculated by normalizing into working electrode geometric surface area. A large strip of carbon felt with 1 cm x 5 cm dimensions served as the counter electrode and a saturated standard calomel electrode was used as a reference electrode. The activity of all synthesized catalyst materials towards OER was examined by recording linear sweep voltammograms (LSV) in 0.5 M NaOH between 1.1 V and 2.1 V vs RHE at a scan rate of 10 mV/s scanned in the anodic direction. Prior to the activity measurements, cyclic voltammograms were recorded for all aforementioned catalysts in N<sub>2</sub> sat. 0.5 M NaOH, at scan rates of 20 mV/s for 10 cycles or until a stable CV was obtained. All the measured potentials were converted into RHE based on the pH of the solution (13.7). Additionally, the built-in IR compensation technique (PEIS-ZIR) was used to measure the uncompensated resistance of the cell and to compensate 85% of the measured cell resistance.

## RESULTS AND DISCUSSION

The catalyst was obtained by outfitting a carbon felt, which acts as a mechanically and chemically robust, highly porous, conductive, flexible 3D framework, with a nanostructured functional coating. Our fabrication process is based on a succession of scalable, wet-chemical deposition reactions solely requiring submerging the felt substrate into different aqueous solutions, alternated by washing steps. Figure 1 summarizes the involved deposition reactions. Prior to seeding, the carbon felt was oxidized with aqua regia. This ensures a pronounced hydrophilicity and thus efficient wetting, and furthermore provides a high density of polar anchoring groups for Sn<sup>2+</sup> adsorption, which supplies the carbon surface with reducing qualities. Without the *aqua regia* treatment, seeding and electroless metallization of graphite felt was found to be severely hampered.<sup>23</sup>

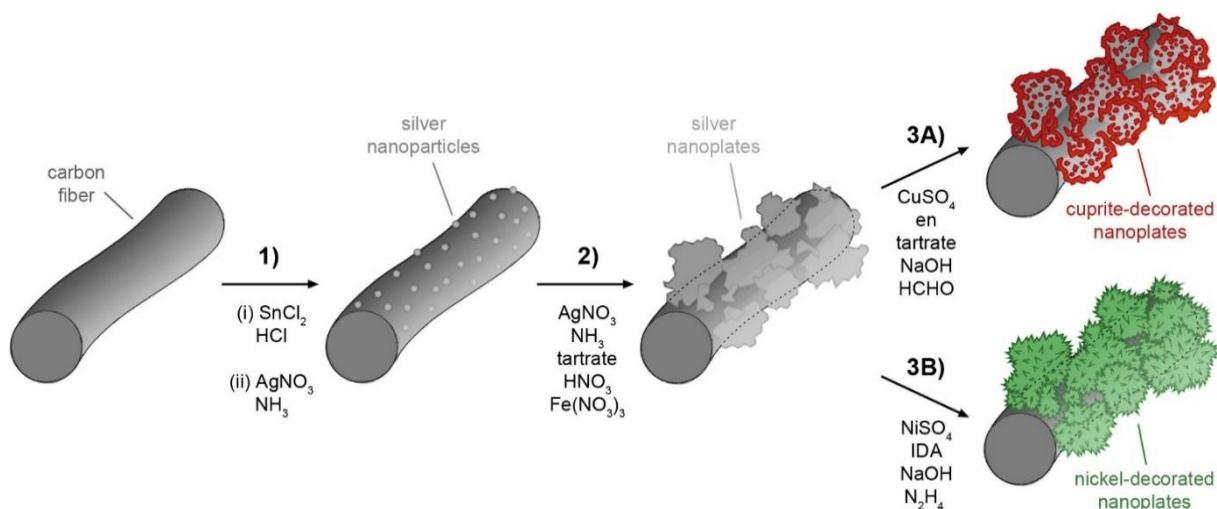


**Figure 1.** Scheme of the catalyst electrode fabrication, indicating the deposition steps, the components of the corresponding reaction solutions, as well as the deposit type.

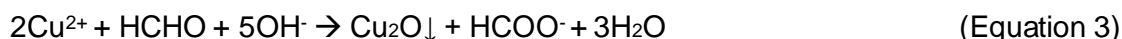
In the first step, the fibers of the carbon felt were decorated with Ag nanoparticles by applying a dual sensitization/activation treatment.<sup>23, 25, 28</sup> In the subsequent electroless plating reaction, the nanoparticles act as nuclei for the nanoplate growth. The Ag nanoparticles are introduced by the reaction of adsorbed Sn<sup>2+</sup> ions with an ammoniacal Ag<sup>+</sup> solution, according to Eq. 1:



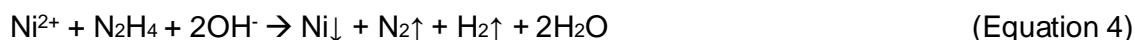
The second step comprises the electroless deposition of Ag nanoplates, which utilizes mixed Fe-tartrate-hydroxide complexes as shape-directing agent.<sup>21</sup> Mechanistically, the reaction can be categorized as an autocatalytic growth of shape-controlled metal nanocrystals on the seeded substrate. It allows for a direct functionalization of the 3D electrode and makes redundant the binders which are commonly required to stabilize coatings derived from colloidal nano-objects.<sup>29</sup> While the chemistry of tartrate-based electroless silver plating baths is potentially complex and not yet fully clarified, we hypothesize that silver reduction involves the initial oxidation of the  $\alpha$ -hydroxy group of the tartrate reducer,<sup>19</sup> resulting in the formation of a ketocarboxylate:



In the third step, the silver nanoplates were modified by secondary electroless plating baths to yield two hetero-nanostructure variants, which were enriched with either Cu or Ni. Interestingly, applying our electroless copper nano plating procedure<sup>30</sup> to Ag nanoplates at slightly elevated temperatures resulted in the formation of cuprous oxide deposits.<sup>21</sup> In this case, the Cu<sup>2+</sup> precursor is only partially reduced to Cu<sup>+</sup>, and the pronounced hydrogen evolution typical for electroless Cu plating is not observed.<sup>31</sup> Thus, we propose the following reaction equation, with hydroxide and tartrate acting as likely Cu<sup>2+</sup> ligands in our system:



Electroless nickel plating was performed using N<sub>2</sub>H<sub>4</sub> as the reducing agent in conjunction with the polyaminocarboxylate chelator IDA to prevent Ni(OH)<sub>2</sub> precipitation, ensure the required plating bath metastability and promote anisotropic growth.<sup>22</sup> Hydrazine-based electroless nickel plating operates under hydrogen and nitrogen evolution, and equation 3 was suggested to account for the observed recombination of hydrogen atoms and their release as gas:<sup>32</sup>



The morphology and bulk composition of the silver nanoplate covered carbon felt and the hetero-nanostructures derived thereof was investigated with SEM-EDS (Figure 2). It is immediately apparent that the surface area of the comparably smooth carbon fibers is greatly increased by the rough, porous Ag coating. This surface structuring both in the micro- (lateral plate dimensions) and in the nanoscale (plate thickness) provides ample, easily accessible surfaces for electrocatalytic experiments (Figure 2a-c). Due to their extended 2D morphology, Ag nanoplates provide undisturbed in-plane paths for efficient electrical conduction and enhanced mechanical stability during bending,<sup>33-34</sup> both of which benefit our target application as high surface area support structure in electrocatalysis. On the other hand, the macroscale structure of the felt offers a high degree of open porosity with a predominance of large macropores, ensuring straightforward mass transport to and from the active sites in the fiber coating.

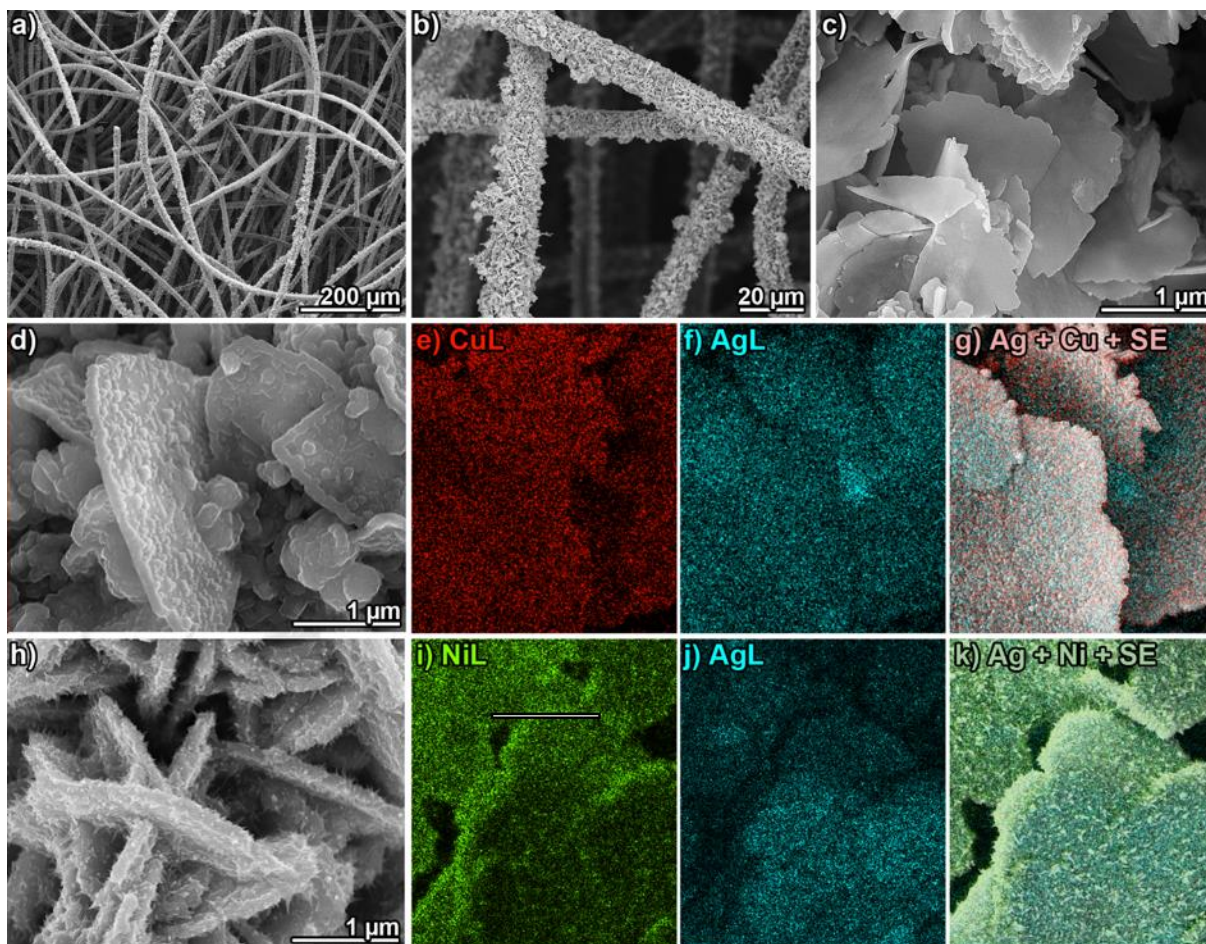


**Figure 2.** (a-c) SEM characterization of the Ag nanoplates coated carbon felt. (d) SEM detail image of Cu nanoparticle decorated Ag nanoplates, and their corresponding EDS maps (e-g). (h) SEM detail image of Ni nanoparticle decorated Ag nanoplates, and their corresponding EDS elemental maps (i-k).

The nanoplates serve as a reliable support for further functionalization, providing nucleation and anchoring points for the growth of secondary materials on their surfaces, particularly on their rugged edges,<sup>21</sup> at which planar defects such as stacking faults surface.<sup>21</sup> Electroless modification of the Ag nanoplates with Cu nanoparticles (Figure 2d-g) or Ni nanoparticle (Figure 2h-k) coatings further increase the surface area of the deposit. Conventional galvanic displacement-based strategies, proceeding under sacrificial oxidation of the nanoplates tend to result in precipitation of poorly soluble salts such as AgCl due to dissolution and mixing with the deposit.<sup>35</sup> Our derivatization reactions yield core-shell hetero-architectures, since the standard reduction potential of the Ag support is considerably more positive compared to Cu and Ni, and the deposit precursors are converted by the dissolved reducing agents rather than by the nanoplates. In accordance with previous results, the Cu nanoparticles preferably nucleate at the highly reactive edges of the silver nanoplates,<sup>21</sup> but also partially cover the basal {111} faces. A similar pattern is found for the nickel nanoparticle. In both cases, the combined SEM/EDS characterization confirms a homogeneous and dense, almost full coverage of the underlying silver nanoplates by the shell materials (Figure 2d-k).

By EDS and XRD, as shown in Figure 3, the bulk composition and the crystallographic orientation of the synthesized nanostructures were further examined. EDS analysis (Figure 3a) confirmed the successful formation of bimetallic surfaces and the decoration of the surface of the Ag nanoplates with either Cu particles (in case of AgCu; 76% Ag and 24% Cu) or Ni nanopikes (in case of AgNi; 37% Ag and 63% Ni). The crystalline nature of the as-synthesized nanostructured materials was verified by XRD, as displayed in Figure 3b. All the as-prepared materials (i.e., Ag, AgCu and AgNi) exhibited five strong reflections at 38°, 44.2°, 64.5°, 77.6° and 81.7° assigned to various crystal planes (i.e., (111), (200), (220), (311) and (222)) of the Ag face-centred cubic crystal structure. Additionally, AgCu and AgNi showed additional reflections for cuprite and metallic nickel as assigned in Figure 3b. AgCu exhibited additional weak peak at 50.4° which can be assigned to bulk metallic Cu.

It is worth to mention here that no shift in the Ag peak positions was observed, indicating that the syntheses work in an additive fashion, and that phases coexist as bimetallic surfaces instead of alloys. Furthermore, the XRD patterns of the materials measured after the OER electrocatalysis do not show significant differences in the peak positions associated with Ag and Ni in both pure Ag and AgNi. The observed CuO in case of AgCu could be attributed to the oxidation of Cu<sub>2</sub>O to CuO since the XRD were collected in air (Figure S2).

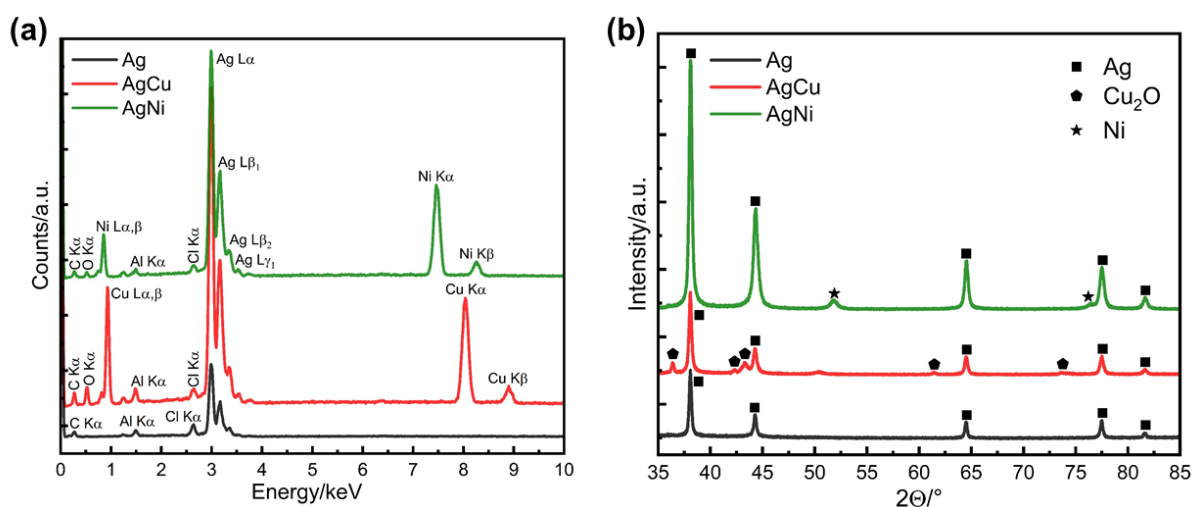


**Figure 3.** (a) EDS spectra and (b) XRD patterns of as-synthesized Ag (black line), AgCu (red line) and AgNi (green line) decorated carbon felts.

The nanoscale architecture of the decorated carbon fibers with AgNi nanoplates, showing the best OER activity, was investigated in more detail using TEM-EDS (Figure 4). To corroborate the synthetically anticipated core-shell architecture of the overcoated nanoplates, we performed TEM analysis on microtome cross-sections of our materials (Figure 4). Whereas the brittle carbon fibers experienced deformation and cracking (Figure 4a&d)), the structure of the catalyst layer was well preserved, revealing a homogeneous coating containing plentiful nanoplates which have grown out of the seed layer and in cross-section appear as bands.

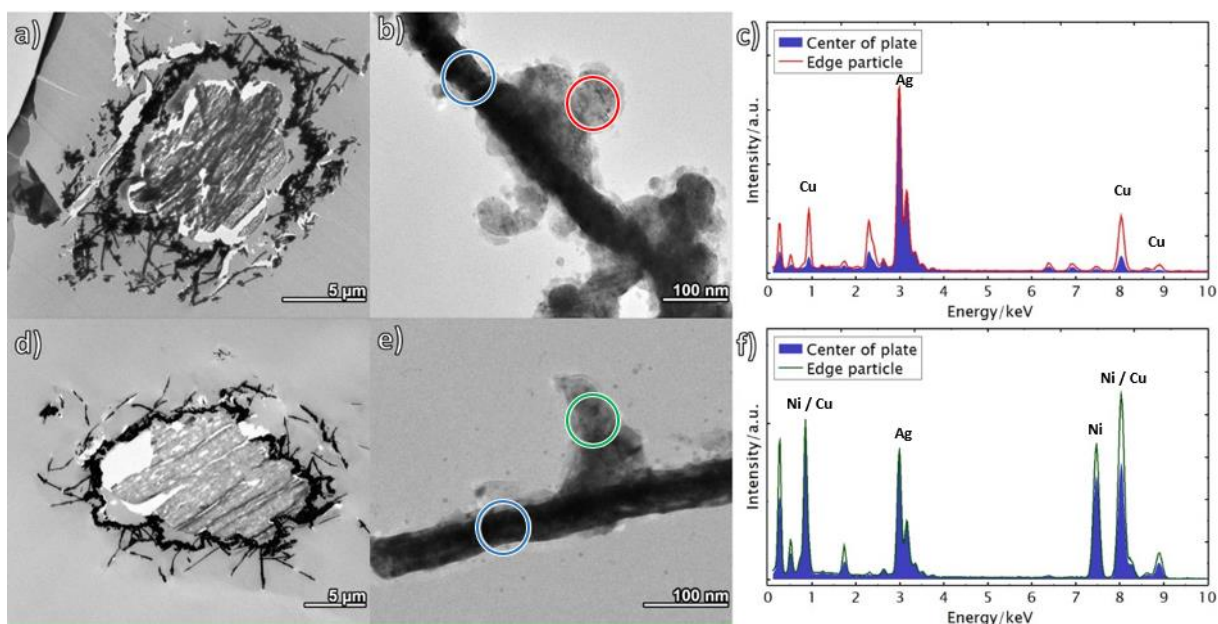


**Figure 4.** Acquired TEM micrographs and corresponding EDS spectra of functionalized Ag nanoplates with Cu (a-c) and with Ni (d-e). (a,d) TEM images of cross section cuts of carbon fiber decorated with (a) Cu-functionalized Ag nanoplates and (d) Ni-functionalized Ag nanoplates. (b,e) detailed TEM image of (b) Cu-functionalized Ag nanoplate and (e) Ni-functionalized Ag nanoplates. (c,f) EDS spectra of marked areas in image b and e, respectively. The EDS spectra are normalized to each other using the silver  $L_{\alpha}$  peak at 2.98 eV for better comparability. The detailed TEM images of the cut Ag nanoplates confirm their coverage by secondary deposits (Cu and Ni in case of AgCu and AgNi).

Detail images of cut nanoplates confirm their coverage by secondary deposits (Figure 4b&e), which possess morphologies matching the SEM results (Figure 2d&h). Local energy-dispersive X-ray spectra show Ag from the nanoplate support as well as Cu and Ni from the modification reactions, the latter being enriched at exposed areas such as nanoplate edges or outgrowths (Figure 4c&f) but are distributed over the complete nanoplate surfaces. EDS analysis confirms the core-shell architecture of the material, showing large Ag contributions in the center of the filaments, which are dominated by the Ag nanoplates, and an inverted Ag-M (Ni and Cu) ratio at the filament edges where the Ni nanospikes and Cu nanoparticles have been deposited.

Electrochemical behaviour of the AgNi and AgCu decorated carbon fibers were investigated next to learn more about the surface species. As seen in Figure S3a, Ag decorated carbon fibers exhibited two major broad oxidation peaks attributed to the oxidation of Ag into  $Ag_2O$  (A1) and the further oxidation of  $Ag_2O$  into AgO (A2). These two oxidation peaks are followed by two reduction peaks; C1 assigned to the reduction of  $Ag_2O$  into Ag and C2 associated with the reduction of AgO into  $Ag_2O$ .<sup>36</sup> Interestingly, AgCu electrodes exhibited additional peaks for the different copper oxidation states; A3/C3 (Cu/Cu<sub>2</sub>O redox species) and A4/C4 (Cu<sub>2</sub>O/CuO redox couple transformation),<sup>37</sup> as shown in Figure S3a. The same behaviour is observed for the AgNi electrode, indicating that the silver surface isn't completely decorated or blocked by the deposition of the second metals (Cu and Ni). Consequently, both the Ag and secondary deposits (i.e., Ni and Cu particles) are electrochemically accessible surface-active sites.

The electrochemically active surface area for Ag nanoplates was measured by Pb underpotential deposition technique<sup>38</sup>, as displayed in Figure S3b. The Ag nanoplate decorated carbon fibers exhibited the highest Ag electrochemically active surface area (198 cm<sup>2</sup>), while AgCu and AgNi showed 108 cm<sup>2</sup> and 40 cm<sup>2</sup> electrochemically active surface Ag

sites, respectively. This introduces additional evidence that both Ag and the secondary deposit metals are electrochemically surface accessible sites.

The performance of the as synthesized materials was tested for OER in 0.5 M NaOH aqueous solution using three-electrode electrochemical cell. The obtained OER performance of the bimetallic materials (AgNi and AgCu) was compared to that of their single components (i.e., Cu, Ni and Ag) and to the commercial Pt/C (40 wt.%) and IrO<sub>2</sub> (40 wt.%) based electrocatalysts. As shown in Figure 5, the bimetallic silver based nanoplates (AgCu and AgNi) exhibited a superior activity and stability towards OER compared to their single components (pure Ag, Cu and Ni), highlighting the enhancing role of the synergistic effect of the bimetallic surfaces. Indeed, AgNi exhibited the best OER electrocatalytic activity among all studied electrocatalysts, as demonstrated by its lowest onset potential (~1.46 V vs. RHE) associated smallest needed overpotential (~0.27 V) to obtain a current density of 10 mA/cm<sup>2</sup>, as shown in Fig.5. It is worth to mention here that the observed peak at ~1.4 V (vs. RHE) for the AgNi can be assigned for the nickel oxide/hydroxide transformation (Ni<sup>II</sup>(OH)<sub>2</sub> / Ni<sup>III</sup>OOH)<sup>39</sup>. This can be evidenced from Figure S3, where the decorated CF with nickel nanoparticles or AgNi exhibited a redox couple around 0.4 V vs SCE (~1.4 V vs. RHE) for Ni<sup>II</sup>(OH)<sub>2</sub> / Ni<sup>III</sup>OOH transformation. Similarly, the seen peak at ~1.6V for AgCu can be assigned for the oxidation of Ag<sub>2</sub>O into AgO<sup>38</sup>.

It is well known that costly commercial Ir-based OER catalysts have low stability in highly alkaline medium compared to Ni, Cu and Ag. For instance, Vass et al<sup>40</sup> investigated the stability of the Ni- and Ir-based anodes under alkaline conditions. They found that Ir dissolution starts at 1.1 V (vs. RHE) and its dissolution rate increases with the increase of the potential, especially with the onset of OER at 1.5 V (vs. RHE). On the other hand, they did not detect any observable dissolution for Ni-based anode under similar conditions. In this regards, high stability of the Ni-based catalysts in alkaline medium is expected. The synthesized AgNi in this study showed high stability under continuous OER in alkaline medium. The good activity of AgNi nanoplates is apparent by the higher current density at certain overpotential. For instance, AgNi nanoplates exhibited ~16 mA/cm<sup>2</sup> at ~1.6 mV (vs. RHE), which is ~5, ~3, and ~20 fold higher than that of Cu, Ni and Ag electrodes, respectively. Additionally, AgNi and AgCu nanoplates showed better (or comparable) activity compared to many previously reported Cu-, Ag- and Ni-based electrodes. This observed enhancement of AgNi nanoplates' activity could be attributed to their smaller charge transfer resistance, as shown in Figure 6a, and/or the key role of Ag in increasing surface-active sites of the nickel most active OER species, β-NiOOH (c.f., Figure 7 and its related discussion)<sup>39</sup>. Our catalyst showed a better or a comparable OER activity to the previously published Ni-based electrocatalyst materials, see Table S1

Furthermore, AgNi nanoplates showed a satisfactory stability compared to Ni nanoplates decorated carbon fibers, as shown in Figure 6b, where the onset potential of OER at AgNi unchanged even after 500 LSVs at 10 mV/s scan rate. On the other side, Ni nanospikes performance towards OER reduces with time as demonstrated by the positive shift of the OER onset potential with time. Additionally, there is no significant changes were detected in the morphology of both bimetallic catalysts after OER electrolysis, see Figure S3.

Glovebox assisted XPS analysis was performed to learn more about the surface-active species of the studied materials (Ag, AgNi and AgCu) while avoiding oxidation due to air exposure after electrochemical testing. Figure S4 and S5 show the overall survey of Cu, Ni, Ag, AgCu and AgNi coated CF before and after OER electrolysis for two hours. Interestingly, bimetallic AgCu and AgNi showed a very weak Ag peak before OER, while after OER the Ag surface amount

significantly increased (see Figure S5-S7). Before OER, the as-prepared AgNi and AgCu resemble a core-shell structure where the surface Ni and Cu act as a decoration while the Ag nanoplates are buried below the surface, thus a very weak Ag 3d signal is observed (see Fig. S6) that corresponds to Ag abundance of 1.1 and 2.6 at.% in the AgNi and AgCu, respectively (Table S3). After OER, the applied oxidative bias during the OER electrocatalysis causes the Ag to emerge on the surface indicated by observation that the Ag content increases to 74.4 and 70.6 at.% in the AgNi and AgCu, respectively.

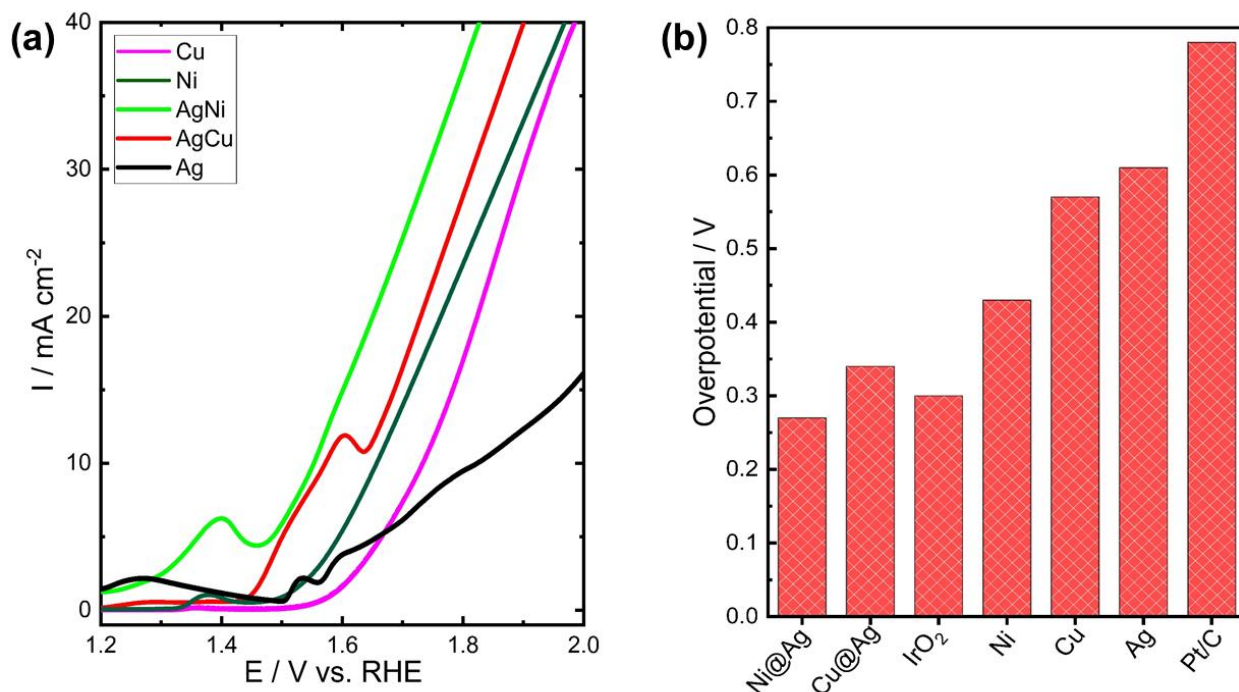


**Figure 5.** (a) OER LSVs of Ag, Cu, Ni, AgCu and AgNi in 0.5 M NaOH at scan rate of 10 mV/s. (b) Comparison of the required overpotential to obtain 10 mA/cm<sup>2</sup> of the various prepared materials.

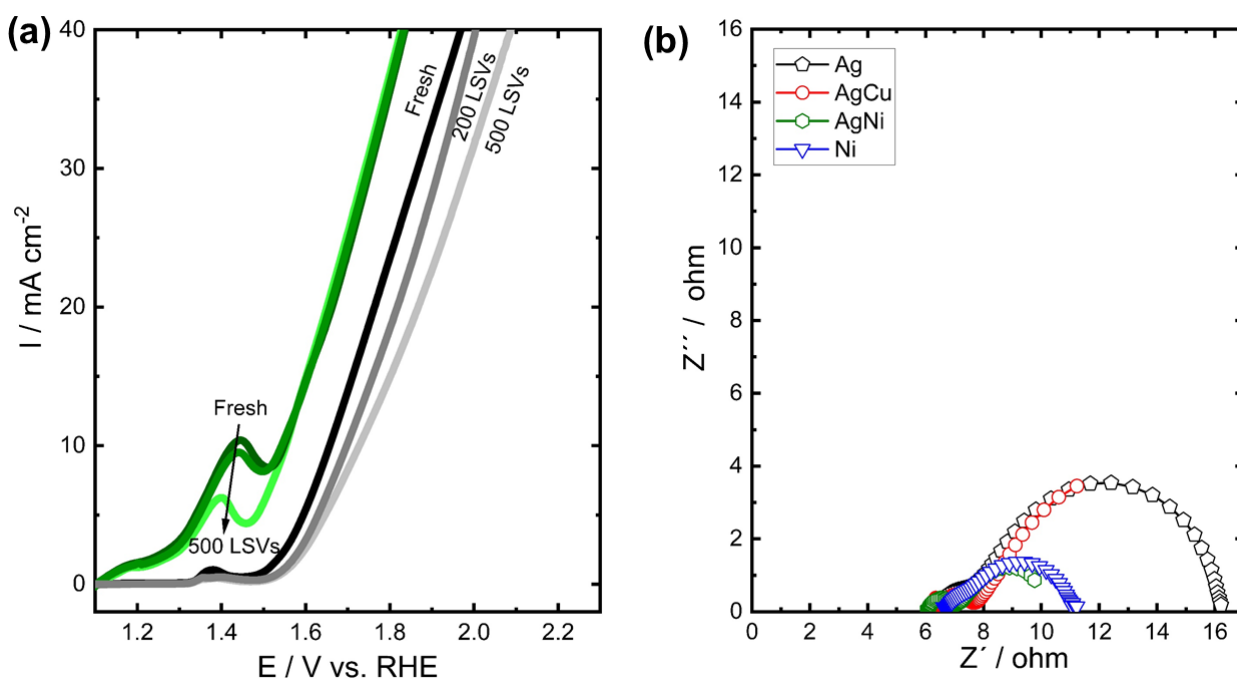


**Figure 6. (a)** LSVs of AgNi (green lines) and Ni (black-grey lines) modified CF electrodes measured after continuous measuring of LSVs (200 and 500) in 0.5 M NaOH at 10 mV/s potential scan and **(b)** Nyquist plots of Ag, AgCu, AgNi and Ni electrodes.

Figure 7 displays the high-resolution XPS spectra of Ni 2p and Cu 2p of AgNi and AgCu catalysts, respectively, compared to pure Ni and Cu electrodes. As seen in this figure, these catalyst materials showed a quite different their surface speciation before and after OER. Both Ni and AgNi decorated CF electrodes showed mixture of metallic Ni (48 at.% Ni for Ni@CF vs 39 at.% for AgNi) and NiO (52 at.% for Ni@CF vs 61 at.% for AgNi) before OER, see Table S4. Interestingly, all nickel surface species (Ni and NiO) of AgNi electrode are completely transformed into the most active nickel phase for OER ( $\beta$ -NiOOH) after OER, while mixture of  $\beta$ -NiOOH (55 at.%) and  $\beta$ -Ni(OH)<sub>2</sub> (45 at.%) is detected for Ni@CF electrode, see Table S4. It is worth to mention here that we could not detect the presence of  $\beta$ -NiOOH phase for AgNi or Ni@CF electrodes from XRD measurements after OER probably due to its amorphous nature and its abundance on the surface of the material rather than in the bulk (Figure S3). For the AgCu samples, there is no change observed in the copper surface species before and after the OER electrocatalysis since the surface of the as-prepared material resembles fully oxidized Cu(II) species, see Table S5. On the other hand, AgCu showed mixture of metallic and oxidized (Cu(II)) copper surface species before OER, but only Cu(II) species after OER.

Even though the Ag species are the main surface fraction with quite similar abundance in both AgNi and Ag@CF materials, examined 'post-mortem', there is a significant difference in the OER electrocatalytic activity in favour of the Ni decorated Ag nanoplates (Figure 6). Namely this material outperforms all examined materials, while the Ni decorated one show activity that is comparable to commercial IrO<sub>2</sub> (see Figure 6). Having in mind the previous statements, we believe that the presence of Ag is significantly affecting the processes of complete transformation of the Ni/NiO species into NiOOH under oxidative bias in alkaline environment,<sup>41-42</sup> which only partially occurs in the case of the pristine Ni@CF. Therefore, according to our XPS results the  $\beta$ -NiOOH phase as an exclusive Ni species on the surface of AgNi have a key role in the OER electrocatalysis performance of this material. However, it is not completely clear whether the  $\beta$ -NiOOH undergoes a transformation into  $\gamma$ -NiOOH under oxidative bias, since according to some reports in the literature, this phase is believed to be the true active OER electrocatalyst in neutral and near neutral environment.<sup>43</sup> Even though from our high-resolution Ni 2p XPS results, no evidence of  $\gamma$ -NiOOH phase was observed on the surface of the AgNi electrocatalyst after OER, we cannot rule out the possibility that it may exist under the oxidative bias and transform back to the  $\beta$ -NiOOH phase when the bias is removed. Moreover, another report states that in alkaline environment the  $\beta$ -NiOOH can be generated from the  $\gamma$ -NiOOH phase via electrochemical aging, yet it is still an open question since under operando OER conditions an unidentified oxide phase was observed.<sup>44</sup> Thus, the resolving of the actual OER active phase together with the possibility of synergistic effect of both Ni and Ag species on the OER activity remain open for discussion. Naturally another question will rise whether the presence of Ag is affecting the lattice peroxide<sup>43</sup> or deprotonation<sup>45</sup> mechanisms that are proposed for OER on NiOOH surfaces. Both possible Ag-Ni synergistic effect and changes in the OER mechanism could be better understood via application of spectro-electrochemical studies under operando conditions.

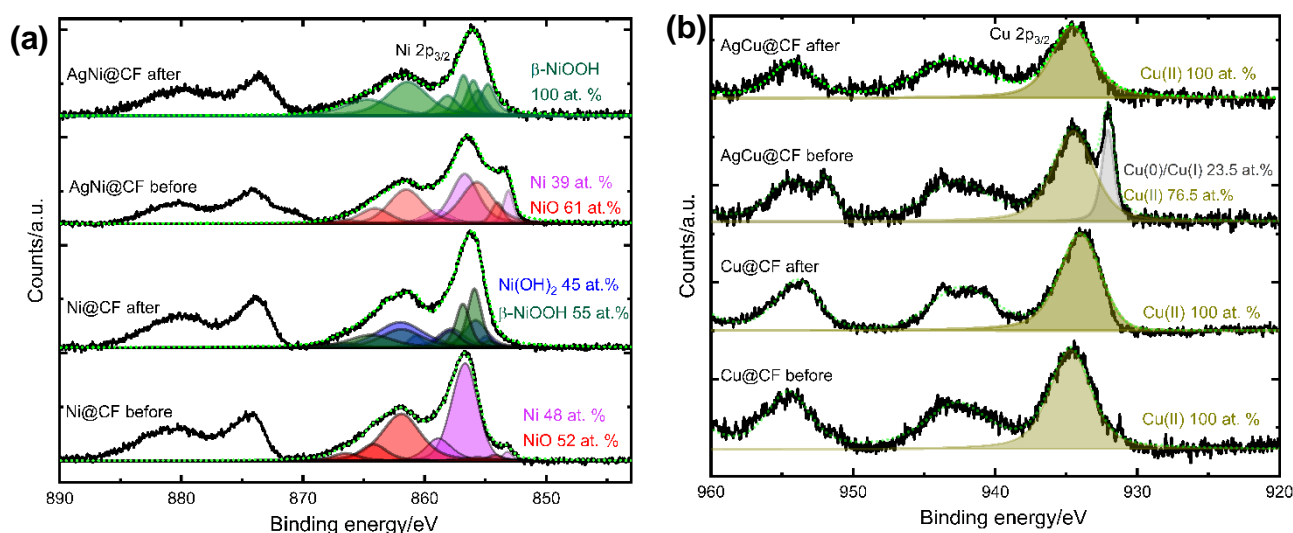


**Figure 7.** High-resolution XPS spectra before and after OER electrocatalysis on AgNi and AgCu, and pristine Ni and Cu coated on carbon felt (CF). (a) Ni 2p<sub>3/2</sub> and (b) Cu 2p<sub>3/2</sub> core levels.

## CONCLUSION

In this work, we establish shape controlled electroless plating as a modular platform for creating freestanding hierarchical multi-component nanostructures as functional electrocatalyst for OER. A simple electroless plating approach was used to decorate commercial carbon fibers with homogeneous coatings of bimetallic AgNi and AgCu nano architectures. AgNi and AgCu decorated carbon fibers showed impressive OER activity and stability comparable to state-of-art Ir-based electrodes. The highest electrocatalytic activity of bimetallic AgNi is attributed to the synergistic effect between Ag and Ni, where the presence of Ag appears to be the key for fully converting the nickel surface species into the most active nickel phase ( $\beta$ -NiOOH).

## Supporting Information.

SI includes additional material and electrochemical characterization of the bimetallic catalysts, such XRD, XPS and SEM.

## ACKNOWLEDGEMENTS

The Helmholtz Association's Initiative and Networking Fund (Helmholtz Young Investigator Group VH-NG-1225) and the Helmholtz Energy Materials Foundry supported this work. The authors acknowledge René Gunder for his help during the GI-XRD measurements. The authors are grateful for Ulrike Kunz for measuring TEM for the as-prepared catalyst materials.

## REFERENCES

(1) Abouserie, A.; El-Nagar, G. A.; Heyne, B.; Günter, C.; Schilde, U.; Mayer, M. T.; Stojkovicj, S.; Roth, C.; Taubert, A. Facile Synthesis of Hierarchical CuS and CuCo<sub>2</sub>S<sub>4</sub> Structures from an Ionic Liquid

- Precursor for Electrocatalysis Applications. *ACS Applied Materials & Interfaces* **2020**, *12* (47), 52560-52570, DOI: 10.1021/acsmi.0c13927.
- (2) Grimaud, A.; Diaz-Morales, O.; Han, B.; Hong, W. T.; Lee, Y.-L.; Giordano, L.; Stoerzinger, K. A.; Koper, M. T. M.; Shao-Horn, Y. Activating lattice oxygen redox reactions in metal oxides to catalyse oxygen evolution. *Nature Chemistry* **2017**, *9* (5), 457-465, DOI: 10.1038/nchem.2695.
- (3) Park, S.; Shao, Y.; Liu, J.; Wang, Y. Oxygen Electrocatalysts for Water Electrolyzers and Reversible Fuel Cells: Status and Perspective. *Energy & Environmental Science* **2012**, *5* (11), 9331-9344, DOI: 10.1039/C2EE22554A.
- (4) Miles, M. H.; Klaus, E. A.; Gunn, B. P.; Locker, J. R.; Serafin, W. E.; Srinivasan, S. The Oxygen Evolution Reaction on Platinum, Iridium, Ruthenium and their Alloys at 80°C in Acid Solutions. *Electrochimica Acta* **1978**, *23* (6), 521-526, DOI: [https://doi.org/10.1016/0013-4686\(78\)85030-0](https://doi.org/10.1016/0013-4686(78)85030-0).
- (5) Jamesh, M.-I.; Sun, X. Recent Progress on Earth Abundant Electrocatalysts for Oxygen Evolution Reaction (OER) in Alkaline Medium to achieve Efficient Water Splitting – A Review. *Journal of Power Sources* **2018**, *400*, 31-68, DOI: <https://doi.org/10.1016/j.jpowsour.2018.07.125>.
- (6) Vij, V.; Sultan, S.; Harzandi, A. M.; Meena, A.; Tiwari, J. N.; Lee, W.-G.; Yoon, T.; Kim, K. S. Nickel-Based Electrocatalysts for Energy-Related Applications: Oxygen Reduction, Oxygen Evolution, and Hydrogen Evolution Reactions. *ACS Catalysis* **2017**, *7* (10), 7196-7225, DOI: 10.1021/acscatal.7b01800.
- (7) Joy, J.; Rajappa, S.; Pillai, V. K.; Alwarappan, S. Co<sub>3</sub>Fe<sub>7</sub>/nitrogen-doped graphene nanoribbons as bi-functional electrocatalyst for oxygen reduction and oxygen evolution. *Nanotechnology* **2018**, *29* (41), 415402, DOI: 10.1088/1361-6528/aad35e.
- (8) Vineesh, T. V.; Sekar, A.; Rajappa, S.; Pal, S.; Alwarappan, S.; Narayanan, T. N. Non-Precious Metal/Metal Oxides and Nitrogen-Doped Reduced Graphene Oxide based Alkaline Water-Electrolysis Cell. *ChemCatChem* **2017**, *9* (22), 4295-4300, DOI: <https://doi.org/10.1002/cctc.201701018>.
- (9) Li, L.; Shao, Q.; Huang, X. Amorphous Oxide Nanostructures for Advanced Electrocatalysis. *Chemistry – A European Journal* **2020**, *26* (18), 3943-3960, DOI: <https://doi.org/10.1002/chem.201903206>.
- (10) Guha, P.; Mohanty, B.; Thapa, R.; Kadam, R. M.; Satyam, P. V.; Jena, B. K. Defect-Engineered MoO<sub>2</sub> Nanostructures as an Efficient Electrocatalyst for Oxygen Evolution Reaction. *ACS Applied Energy Materials* **2020**, *3* (6), 5208-5218, DOI: 10.1021/acsaem.9b02551.
- (11) Suryanto, B. H. R.; Wang, Y.; Hocking, R. K.; Adamson, W.; Zhao, C. Overall Electrochemical Splitting of Water at the Heterogeneous Interface of Nickel and Iron Oxide. *Nature Communications* **2019**, *10* (1), 5599, DOI: 10.1038/s41467-019-13415-8.
- (12) Huan, T. N.; Rousse, G.; Zanna, S.; Lucas, I. T.; Xu, X.; Menguy, N.; Mougél, V.; Fontecave, M. A Dendritic Nanostructured Copper Oxide Electrocatalyst for the Oxygen Evolution Reaction. *Angewandte Chemie International Edition* **2017**, *56* (17), 4792-4796, DOI: <https://doi.org/10.1002/anie.201700388>.
- (13) Santos, A.; Deen, M. J.; Marsal, L. F. Low-Cost Fabrication Technologies for Nanostructures: State-Of-The-Art and Potential. *Nanotechnology* **2015**, *26* (4), 042001, DOI: 10.1088/0957-4484/26/4/042001.
- (14) Zhang, B.; Sun, J.; Salahuddin, U.; Gao, P.-X. Hierarchical and Scalable Integration of Nanostructures for Energy and Environmental Applications: A Review of Processing, Devices, and Economic Analyses. *Nano Futures* **2020**, *4* (1), 012002, DOI: 10.1088/2399-1984/ab75ad.
- (15) Kim, K.; Lee, H.-B.-R.; Johnson, R. W.; Tanskanen, J. T.; Liu, N.; Kim, M.-G.; Pang, C.; Ahn, C.; Bent, S. F.; Bao, Z. Selective Metal Deposition at Graphene Line Defects by Atomic Layer Deposition. *Nature Communications* **2014**, *5* (1), 4781, DOI: 10.1038/ncomms5781.
- (16) Pawar, S. M.; Pawar, B. S.; Kim, J. H.; Joo, O.-S.; Lokhande, C. D. Recent Status of Chemical Bath Deposited Metal Chalcogenide and Metal Oxide Thin Films. *Current Applied Physics* **2011**, *11* (2), 117-161, DOI: <https://doi.org/10.1016/j.cap.2010.07.007>.
- (17) Rao, C. R. K.; Trivedi, D. C. Chemical and Electrochemical Depositions of Platinum Group Metals and their Applications. *Coordination Chemistry Reviews* **2005**, *249* (5), 613-631, DOI: <https://doi.org/10.1016/j.ccr.2004.08.015>.

- (18) Zheng, X.; Smith, W.; Jackson, J.; Moran, B.; Cui, H.; Chen, D.; Ye, J.; Fang, N.; Rodriguez, N.; Weisgraber, T.; Spadaccini, C. M. Multiscale Metallic Metamaterials. *Nature Materials* **2016**, *15* (10), 1100-1106, DOI: 10.1038/nmat4694.
- (19) Muench, F.; Felix, E.-M.; Rauber, M.; Schaefer, S.; Antoni, M.; Kunz, U.; Kleebe, H.-J.; Trautmann, C.; Ensinger, W. Electrodeposition and Electroless Plating of Hierarchical Metal Superstructures Composed of 1D Nano- and Microscale Building Blocks. *Electrochimica Acta* **2016**, *202*, 47-54, DOI: <https://doi.org/10.1016/j.electacta.2016.03.188>.
- (20) Zeng, M.; Wang, H.; Zhao, C.; Wei, J.; Qi, K.; Wang, W.; Bai, X. Nanostructured Amorphous Nickel Boride for High-Efficiency Electrocatalytic Hydrogen Evolution over a Broad pH Range. *ChemCatChem* **2016**, *8* (4), 708-712, DOI: <https://doi.org/10.1002/cctc.201501221>.
- (21) Muench, F.; Vaskevich, A.; Popovitz-Biro, R.; Bendikov, T.; Feldman, Y.; Rubinstein, I. Expanding the Boundaries of Metal Deposition: High Aspect Ratio Silver Nanoplatelets Created by Merging Nanobelts. *Electrochimica Acta* **2018**, *264*, 233-243, DOI: <https://doi.org/10.1016/j.electacta.2018.01.103>.
- (22) Boettcher, T.; Schaefer, S.; Antoni, M.; Stohr, T.; Kunz, U.; Dürrschnabel, M.; Molina-Luna, L.; Ensinger, W.; Muench, F. Shape-Selective Electroless Plating within Expanding Template Pores: Etching-Assisted Deposition of Spiky Nickel Nanotube Networks. *Langmuir* **2019**, *35* (12), 4246-4253, DOI: 10.1021/acs.langmuir.9b00030.
- (23) Muench, F.; Solomonov, A.; Bendikov, T.; Molina-Luna, L.; Rubinstein, I.; Vaskevich, A. Empowering Electroless Plating to Produce Silver Nanoparticle Films for DNA Biosensing Using Localized Surface Plasmon Resonance Spectroscopy. *ACS Applied Bio Materials* **2019**, *2* (2), 856-864, DOI: 10.1021/acsabm.8b00702.
- (24) Yang, K.-C.; Yao, C.-T.; Huang, L.-Y.; Tsai, J.-C.; Hung, W.-S.; Hsueh, H.-Y.; Ho, R.-M. Single Gyroid-Structured Metallic Nanoporous Spheres Fabricated from Double Gyroid-Forming Block Copolymers via Templated Electroless Plating. *NPG Asia Materials* **2019**, *11* (1), 9, DOI: 10.1038/s41427-019-0108-z.
- (25) Mashentseva, A. A. Effect of the Oxidative Modification and Activation of Templates Based on Poly(ethylene terephthalate) Track-Etched Membranes on the Electroless Deposition of Copper and the Catalytic Properties of Composite Membranes. *Petroleum Chemistry* **2019**, *59* (12), 1337-1344, DOI: 10.1134/S0965544119120089.
- (26) Muench, F.; Schaefer, S.; Hagelüken, L.; Molina-Luna, L.; Dürrschnabel, M.; Kleebe, H.-J.; Brötz, J.; Vaskevich, A.; Rubinstein, I.; Ensinger, W. Template-Free Electroless Plating of Gold Nanowires: Direct Surface Functionalization with Shape-Selective Nanostructures for Electrochemical Applications. *ACS Applied Materials & Interfaces* **2017**, *9* (36), 31142-31152, DOI: 10.1021/acsami.7b09398.
- (27) Biesinger, M. C.; Payne, B. P.; Lau, L. W. M.; Gerson, A.; Smart, R. S. C. X-ray Photoelectron Spectroscopic Chemical State Quantification of Mixed Nickel Metal, Oxide and Hydroxide Systems. *Surface and Interface Analysis* **2009**, *41* (4), 324-332, DOI: <https://doi.org/10.1002/sia.3026>.
- (28) Wei, X.; Roper, D. K. Tin Sensitization for Electroless Plating Review. *Journal of The Electrochemical Society* **2014**, *161* (5), D235-D242, DOI: 10.1149/2.047405jes.
- (29) Lee, C.-L.; Syu, C.-M.; Huang, C.-H.; Chiou, H.-P.; Chao, Y.-J.; Yang, C.-C. Cornered Silver and Silverplatinum Nanodisks: Preparation and Promising Activity for Alkaline Oxygen Reduction Catalysis. *Applied Catalysis B: Environmental* **2013**, *132-133*, 229-236, DOI: <https://doi.org/10.1016/j.apcatb.2012.11.038>.
- (30) Muench, F.; Sun, L.; Kottakkat, T.; Antoni, M.; Schaefer, S.; Kunz, U.; Molina-Luna, L.; Dürrschnabel, M.; Kleebe, H.-J.; Ayata, S.; Roth, C.; Ensinger, W. Free-Standing Networks of Core-Shell Metal and Metal Oxide Nanotubes for Glucose Sensing. *ACS Applied Materials & Interfaces* **2017**, *9* (1), 771-781, DOI: 10.1021/acsami.6b13979.
- (31) Van Den Meerakker, J. E. A. M. On the Mechanism of Electroless Plating. I. Oxidation of Formaldehyde at Different Electrode Surfaces. *Journal of Applied Electrochemistry* **1981**, *11* (3), 387-393, DOI: 10.1007/BF00613959.
- (32) Mallory, G. O.; Hajdu, J. B. *Electroless Plating: Fundamentals and Applications*, 1990.

- (33) Lee, Y.-I.; Kim, S.; Jung, S.-B.; Myung, N. V.; Choa, Y.-H. Enhanced Electrical and Mechanical Properties of Silver Nanoplatelet-Based Conductive Features Direct Printed on a Flexible Substrate. *ACS Applied Materials & Interfaces* **2013**, *5* (13), 5908-5913, DOI: 10.1021/am401757y.
- (34) Dang, R.; Song, L.; Dong, W.; Li, C.; Zhang, X.; Wang, G.; Chen, X. Synthesis and Self-Assembly of Large-Area Cu Nanosheets and Their Application as an Aqueous Conductive Ink on Flexible Electronics. *ACS Applied Materials & Interfaces* **2014**, *6* (1), 622-629, DOI: 10.1021/am404708z.
- (35) Yang, C.-C.; Chen, H.-R.; Lee, C.-L. Galvanic Deposition and Electrocatalytic Oxygen Reduction of Standing Pt/AgCl-Coated Ag Nanosheets. *Journal of Solid State Electrochemistry* **2015**, *19* (3), 663-670, DOI: 10.1007/s10008-014-2648-z.
- (36) Abd El Rehim, S. S.; Hassan, H. H.; Ibrahim, M. A. M.; Amin, M. A. Electrochemical Behaviour of a Silver Electrode in NaOH Solutions. *Monatshefte für Chemie / Chemical Monthly* **1998**, *129* (11), 1103-1117, DOI: 10.1007/PL00010123.
- (37) García-Cruz, L.; Ania, C. O.; Carvalho, A. P.; Badosz, T. J.; Montiel, V.; Iniesta, J. The Role of Carbon on Copper–Carbon Composites for the Electrooxidation of Alcohols in an Alkaline Medium. *C* **2017**, *3* (4), 36.
- (38) El-Nagar, G. A.; Sarhan, R. M.; Abouserie, A.; Maticiu, N.; Bargheer, M.; Lauermann, I.; Roth, C. Efficient 3D-Silver Flower-like Microstructures for Non-Enzymatic Hydrogen Peroxide (H<sub>2</sub>O<sub>2</sub>) Amperometric Detection. *Scientific Reports* **2017**, *7* (1), 12181, DOI: 10.1038/s41598-017-11965-9.
- (39) El-Nagar, G. A.; Derr, I.; Fetyan, A.; Roth, C. One-pot synthesis of a high performance chitosan-nickel oxyhydroxide nanocomposite for glucose fuel cell and electro-sensing applications. *Applied Catalysis B: Environmental* **2017**, *204*, 185-199, DOI: <https://doi.org/10.1016/j.apcatb.2016.11.031>.
- (40) Vass, Á.; Kormányos, A.; Kószó, Z.; Endródi, B.; Janáky, C. Anode Catalysts in CO<sub>2</sub> Electrolysis: Challenges and Untapped Opportunities. *ACS Catalysis* **2022**, *12* (2), 1037-1051, DOI: 10.1021/acscatal.1c04978.
- (41) Huang, L. F.; Hutchison, M. J.; Santucci, R. J.; Scully, J. R.; Rondinelli, J. M. Improved Electrochemical Phase Diagrams from Theory and Experiment: The Ni–Water System and Its Complex Compounds. *The Journal of Physical Chemistry C* **2017**, *121* (18), 9782-9789, DOI: 10.1021/acs.jpcc.7b02771.
- (42) Ash, B.; Nalajala, V. S.; Popuri, A. K.; Subbaiah, T.; Minakshi, M. Perspectives on Nickel Hydroxide Electrodes Suitable for Rechargeable Batteries: Electrolytic vs. Chemical Synthesis Routes. *Nanomaterials* **2020**, *10* (9), 1878.
- (43) Li, L.-F.; Li, Y.-F.; Liu, Z.-P. Oxygen Evolution Activity on NiOOH Catalysts: Four-Coordinated Ni Cation as the Active Site and the Hydroperoxide Mechanism. *ACS Catalysis* **2020**, *10* (4), 2581-2590, DOI: 10.1021/acscatal.9b04975.
- (44) Yeo, B. S.; Bell, A. T. In Situ Raman Study of Nickel Oxide and Gold-Supported Nickel Oxide Catalysts for the Electrochemical Evolution of Oxygen. *The Journal of Physical Chemistry C* **2012**, *116* (15), 8394-8400, DOI: 10.1021/jp3007415.
- (45) Diaz-Morales, O.; Ferrus-Suspedra, D.; Koper, M. T. M. The Importance of Nickel Oxyhydroxide Deprotonation on its Activity towards Electrochemical Water Oxidation. *Chemical Science* **2016**, *7* (4), 2639-2645, DOI: 10.1039/C5SC04486C.